

Article

# The Enhanced Intramolecular Energy Transfer and Strengthened ff Luminescence of a Stable Helical Eu Complex in Ionic Liquids

Yuki Hasegawa <sup>1</sup>, Ayumi Ishii <sup>1,2,\*</sup>, Yudai Inazuka <sup>1</sup>, Naho Yajima <sup>1</sup>, Shogo Kawaguchi <sup>3</sup>, Kuniyoshi Sugimoto <sup>3</sup>  and Miki Hasegawa <sup>1,\*</sup> 

<sup>1</sup> Department of Chemistry and Biological Science, College of Science and Engineering, Aoyama Gakuin University, 5-10-1 Fuchinobe, Chuo-ku, Sagami-hara 252-5258, Kanagawa, Japan; y.hasegawa106@gmail.com (Y.H.); zoo-injpn@outlook.com (Y.I.); nahoyng@gmail.com (N.Y.)

<sup>2</sup> JST, PRESTO, 4-1-8 Honcho, Kawaguchi 332-0012, Saitama, Japan

<sup>3</sup> Research & Utilization Division, Japan Synchrotron Radiation Research Institute (JASRI/SPring-8), 1-1-1 Kouto, Sayo 679-5198, Hyogo, Japan; kawaguchi@spring8.or.jp (S.K.); ksugimoto@spring8.or.jp (K.S.)

\* Correspondence: ayumi@chem.aoyama.ac.jp (A.I.); hasemiki@chem.aoyama.ac.jp (M.H.); Tel.: +81-42-759-6220 (A.I.); +81-42-759-6221 (M.H.)

Received: 12 December 2017; Accepted: 17 January 2018; Published: 24 January 2018

**Abstract:** The luminescence of a Eu complex (EuL) is enhanced by stabilization of the coordination structure in highly viscous ionic liquids. The EuL was found to maintain a stable single helical structure both in organic solvents and in the ionic liquids [BMIM][PF<sub>6</sub>] and [EMIM][PF<sub>6</sub>]. A colorless solution of EuL dissolved in [BMIM][PF<sub>6</sub>] exhibits bright red luminescence with a quantum yield of 32.3%, a value that is much higher than that in acetonitrile (12%). Estimated rate constants for the energy relaxation pathway indicate that the energy transfer efficiency is enhanced in [BMIM][PF<sub>6</sub>] as a result of the suppression of molecular fluctuations in the ligands. Additionally, a highly luminescent helical structure is preserved in [EMIM][PF<sub>6</sub>] up to 120 °C.

**Keywords:** Eu complex; ionic liquid; luminescence; energy transfer; molecular fluctuation

## 1. Introduction

Lanthanide (Ln) luminescence originating from electric dipole forbidden ff transitions can be sensitized through intramolecular energy transfer from photo-excited coordinated organic ligands [1,2]. These luminescence properties have received much attention because of their potential in a broad range of applications. The luminescence bands of Ln complexes appear at almost the same positions as those of other coordination compounds, although the luminescence is readily deactivated by molecular vibrations of the ligands or solvent. Therefore, obtaining highly luminescent Ln compounds requires the appropriate design of the organic ligands or the selection of an optimal media [3].

Previously, we have reported a luminescent Ln complex (LnL) having a hexadentate ligand composed of two bipyridine moieties bridged by an ethylenediamine group, which surrounds the center metal in a helical manner. Remarkably, a series of these LnL complexes exhibited high stability, maintaining a single helical molecular structure even in organic solvents such as acetonitrile [4]. EuL produces bright luminescence with a quantum yield of over 50% in the solid state, while the luminescence becomes weakened in acetonitrile (12%) because non-radiative deactivation process is enhanced by molecular fluctuations, especially in the ligand that acts as an energy donor. Very recently, the Hatanaka group determined the reason for this decreased luminescence, based on computational studies of Tb complexes with these same ligands and their derivatives [5]. They demonstrated that the single bond around the bridging and azomethine moieties is drastically transformed in the excited triplet state. These molecular fluctuations appear to be depressed in a high viscosity matrix.

In the present work, we focused on the use of ionic liquids (ILs) as a matrix for luminescent Ln complexes because ILs have been shown to act as unique donor/acceptor solvents [6]. To date, ILs have been used as alternatives for organic solvents in chemical reactions [7–10], extractions [11–13], and spectroscopic studies [14–17] because they have a number of useful properties, including low volatility, nonflammability, high ionic conductivity, and wide electrochemical windows [18,19]. As an example, employing ILs as solvents for spectroscopic studies results in high luminescence quantum yields from Ln ions, in addition to enhanced photostability [20]. In the case of Ln complexes, structural stability is an important aspect of maintaining the strong luminescence of the Ln ions. Thus, a stable Ln complex in an IL matrix could enhance the luminescent properties of the Ln ions.

The goal of this investigation was therefore to enhance Ln luminescence by stabilization of the coordination structure in ILs. Two ILs shown in Figure 1 were selected for use with a luminescent helical Eu complex (abbreviated as EuL): 1-butyl-3-methylimidazolium hexafluorophosphate ([BMIM][PF<sub>6</sub>]), which has a melting point of approximately 10 °C and thus is a liquid at room temperature [21], and 1-ethyl-3-methylimidazolium hexafluorophosphate ([EMIM][PF<sub>6</sub>]), which has a melting point of 65 °C and thus is a solid [22]. Since both ILs have the same counter anion as the EuL, the complex is readily dissolved in these materials. Herein, we report the enhanced emission of EuL in ILs and discuss the associated mechanism based on considering molecular fluctuations, especially those of the ligand that acts as an energy donor.

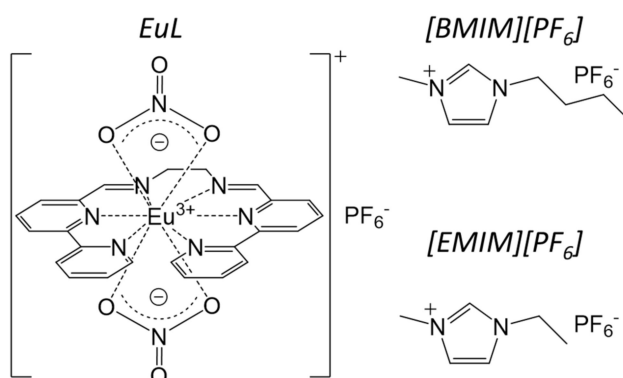


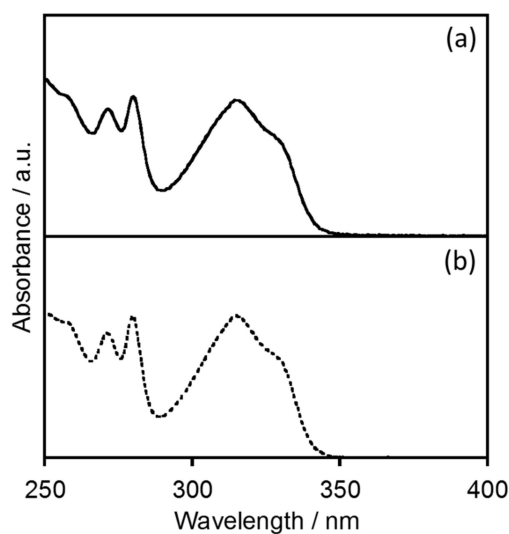
**Figure 1.** Molecular structures of the Eu complex (EuL) and the ionic liquids [BMIM][PF<sub>6</sub>] and [EMIM][PF<sub>6</sub>].

## 2. Results and Discussion

### 2.1. Electronic Structure of EuL in [BMIM][PF<sub>6</sub>]

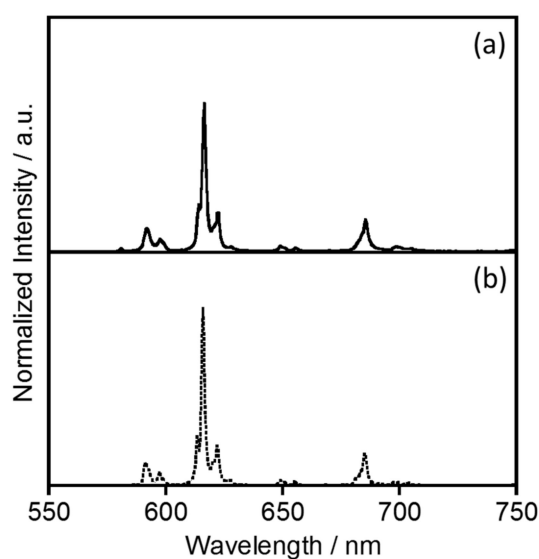
#### 2.1.1. Electronic Absorption and Luminescence Properties

Figure 2 shows the electronic absorption spectrum of EuL in [BMIM][PF<sub>6</sub>], compared with that in acetonitrile [4]. In [BMIM][PF<sub>6</sub>], the EuL generates absorption bands at 271, 280, 315, and 328 nm, assigned to the  $\pi\pi^*$  and  $n\pi^*$  transitions of the ligand. The spectral shape and position observed in [BMIM][PF<sub>6</sub>] are almost consistent with in acetonitrile. The luminescence spectra of EuL in [BMIM][PF<sub>6</sub>] and acetonitrile are provided in Figure 3. The luminescence bands of EuL in [BMIM][PF<sub>6</sub>] are also observed at the same position as in acetonitrile. The luminescence bands at 580, 592, 616, 649, and 686 nm are assigned to the  $^5D_0 \rightarrow ^7F_0$ ,  $^5D_0 \rightarrow ^7F_1$ ,  $^5D_0 \rightarrow ^7F_2$ ,  $^5D_0 \rightarrow ^7F_3$ , and  $^5D_0 \rightarrow ^7F_4$  transitions of Eu<sup>3+</sup>, respectively ( $\lambda_{\text{ex}} = 328$  nm). These spectral data indicate that the coordination structure of EuL in acetonitrile is maintained in [BMIM][PF<sub>6</sub>]. This is supported by the luminescence lifetime ( $\tau_{\text{obs}}$ ) of EuL in [BMIM][PF<sub>6</sub>], which is almost the same as in acetonitrile (Table 1 and Figure S1.)



**Figure 2.** Electronic absorption spectra of the helical Eu complex with L (a) in [BMIM][PF<sub>6</sub>] compared with (b) in acetonitrile [4].

The excitation spectra monitored at these emission bands (Figure S2) correspond to the absorption bands positions of the ligand in Figure 1, demonstrating that intramolecular energy transfer from the ligand to Eu<sup>3+</sup> takes place in [BMIM][PF<sub>6</sub>]. Interestingly, the luminescence quantum yield ( $\phi_{ff}$ ) of EuL in [BMIM][PF<sub>6</sub>] is much higher than that in acetonitrile (Table 1). Thus, energy transfer from the ligand to Eu<sup>3+</sup> evidently proceeds much more efficiently in [BMIM][PF<sub>6</sub>] than in acetonitrile.



**Figure 3.** Emission spectra of the helical Eu complex with L (a) in [BMIM][PF<sub>6</sub>] compared with (b) in acetonitrile [4] ( $\lambda_{ex} = 328$  nm).

**Table 1.** Luminescence quantum yields ( $\phi_{ff}$ ) and luminescence lifetimes ( $\tau_{obs}$ ) of the helical Eu complex with L in [BMIM][PF<sub>6</sub>] and in acetonitrile [4] (<sup>a</sup>:  $\lambda_{ex} = 328$  nm,  $\lambda_{mon} = 550$ – $782$  nm, <sup>b</sup>:  $\lambda_{ex} = 340$  nm,  $\lambda_{mon} = 616$  nm).

	$\phi_{ff}$ (%) <sup>a</sup>	$\tau_{obs}$ (ms) <sup>b</sup>
in [BMIM][PF <sub>6</sub> ]	32.3	1.48
in acetonitrile	12.0	1.55

### 2.1.2. Energy Transfer Efficiency

The luminescence efficiency [1] of  $\text{Eu}^{3+}$  sensitized by the ligand ( $\phi_{\text{ff}}$ ) is determined by the triplet yield of the ligand ( $\phi_{\text{ISC}}$ ), the efficiency of the energy transfer ( $\eta_{\text{EnT}}$ ), and the efficiency of the metal-centered luminescence ( $\eta_{\text{Ln}}$ ), as follows:

$$\phi_{\text{ff}} = \phi_{\text{ISC}} \times \eta_{\text{EnT}} \times \phi_{\text{Ln}}. \quad (1)$$

Based on the  $n\pi^*$  character of the ligand and the high spin-orbit coupling constants of the lanthanide ion, a  $\phi_{\text{ISC}}$  value of approximately 1 can be assumed. The value of  $\phi_{\text{Ln}}$  can then be calculated from the experimentally observed emission lifetime ( $\tau_{\text{ff}}$ ) and the radiative rate constant ( $k_{\text{R}}$ ) of the lanthanide ion, as shown below:

$$\phi_{\text{Ln}} = k_{\text{R}} \times \tau_{\text{ff}}. \quad (2)$$

The  $k_{\text{R}}$  value of the emissive excited state,  ${}^5\text{D}_0$ , is the sum of the spontaneous emission probabilities,  $A_J(0, J)$ , to the lower  ${}^7\text{F}_J$  levels in  $\text{Eu}^{3+}$ , and can in turn be calculated using the following equation:

$$k_{\text{R}} = \sum A_J(0, J) = A_{\text{MD}} \times \sum A_{\text{ED}}. \quad (3)$$

Here, the spontaneous emission probability of the magnetic dipole  ${}^5\text{D}_0 \rightarrow {}^7\text{F}_1$  transition,  $A_{\text{MD}}$ , is virtually independent of the ligand field or the environment of the ions, and can be determined directly from the theoretically calculated dipole strength as follows:

$$A_{\text{MD}} = \frac{64\pi^4 \sigma_{\text{MD}}^3 n^3}{3h(2J+1)} \times S_{\text{MD}}. \quad (4)$$

In the above,  $\sigma_{\text{MD}}$  is the energy gap between the excited ( ${}^5\text{D}_0$ ) and final ( ${}^7\text{F}_1$ ) states (with a value of  $16,949.2 \text{ cm}^{-1}$ ),  $n$  is the refractive index (1.41 for [BMIM][PF<sub>6</sub>] and 1.34 for acetonitrile [23,24]), and  $S_{\text{MD}}$  is the magnetic dipole strength. The latter parameter has been calculated theoretically for the  ${}^5\text{D}_0 \rightarrow {}^7\text{F}_1$  transition of  $\text{Eu}^{3+}$  and found to have a value of  $9.60 \times 10^{-42} \text{ esu}^2 \text{ cm}^2$ , resulting in a value of  $37.93 \text{ s}^{-1}$  for  $A_{\text{MD}}$ .

$A_{\text{ED}}$  in Equation (3) is the emission probability associated with the electric dipole transition, as determined using the Judd–Ofelt parameter ( $\Omega_{\lambda}$ ) in the equation below:

$$A_{\text{ED}} = \frac{64\pi^4 e^2 \sigma_J^3}{3h(2J+1)} \frac{n(n^2+2)^2}{9} \times \sum_{\lambda=2,4} \Omega_{\lambda} \left| \langle \psi_J \| U^{(\lambda)} \| \psi'_{J'} \rangle \right|^2. \quad (5)$$

$\Omega_{\lambda}$  is, in turn, calculated from the following equation:

$$\Omega_{\lambda} = \frac{S_{\text{MD}} \sigma_{\text{MD}}^3}{e^2 \sigma_J^3} \frac{9n^2}{(n^2+2)^2} \frac{\int I_J(\nu) d\nu}{\left| \langle \psi_J \| U^{(\lambda)} \| \psi'_{J'} \rangle \right|^2 \int I_{\text{MD}}(\nu) d\nu}. \quad (6)$$

Here,  $\int I_J d\nu / \int I_{\text{MD}} d\nu$  is the ratio of the integrated intensity of the corrected  $\text{Eu}^{3+}$  luminescence spectrum ( ${}^5\text{D}_0 \rightarrow {}^7\text{F}_J$ ;  $J = 0, 1, 2, 3,$  and  $4$ ) to the intensity of the  ${}^5\text{D}_0 \rightarrow {}^7\text{F}_1$  band, and  $|\langle \Psi_J \| U^{(\lambda)} \| \Psi'_{J'} \rangle|$  is the tensor operator [25]. The  $\Omega_2$  and  $\Omega_4$  values are greatly affected by the ligand field symmetry around the  $\text{Eu}^{3+}$  ion, and the values for EuL in [BMIM][PF<sub>6</sub>] are estimated as  $7.03 \times 10^{-20}$  and  $5.80 \times 10^{-20} \text{ cm}^2$ , respectively. These values are almost the same as in acetonitrile ( $\Omega_2 = 7.82 \times 10^{-20} \text{ cm}^2$ ,  $\Omega_4 = 5.99 \times 10^{-20} \text{ cm}^2$ ), indicating that the ligand field symmetry of EuL is maintained in [BMIM][PF<sub>6</sub>]. Based on the Judd–Ofelt analysis, we can estimate  $A_{\text{ED}}$  to be  $365.6 \text{ s}^{-1}$  for the  ${}^5\text{D}_0 \rightarrow {}^7\text{F}_2$  transition and  $123.1 \text{ s}^{-1}$  for the  ${}^5\text{D}_0 \rightarrow {}^7\text{F}_4$  transition in [BMIM][PF<sub>6</sub>], using the  $k_{\text{R}}$  value

of  $287.2 \text{ s}^{-1}$  obtained from Equation (3). The non-radiative rate constant ( $k_{\text{NR}}$ ) can be estimated using the relationship below:

$$k_{\text{NR}} = \frac{1}{\tau_{\text{obs}}} - k_{\text{R}}. \quad (7)$$

In [BMIM][PF<sub>6</sub>], the  $k_{\text{NR}}$  value for the emissive <sup>5</sup>D<sub>0</sub> excited state is  $388.5 \text{ s}^{-1}$ , which is comparable to that in acetonitrile. Thus, the effect of the solvent on the non-radiative processes of the Eu<sup>3+</sup> ion is also equivalent between [BMIM][PF<sub>6</sub>] and acetonitrile.

Interestingly, the  $\eta_{\text{EnT}}$  value calculated using Equations (1) and (2) is 76.0% in [BMIM][PF<sub>6</sub>], which is significantly larger than that in acetonitrile (29.1%). It is well known that the energy transfer process in Ln complexes is significantly affected by the energy donor level and by the distance between the metal and ligand. In the present work, the latter effect may be negligible since the ligand field symmetry around the Eu<sup>3+</sup> ion appears to be independent of the solvent, meaning that the electric structure of the ligand in [BMIM][PF<sub>6</sub>] may enhance the energy transfer efficiency in the IL compared to that in acetonitrile.

### 2.1.3. Estimation of the Energy Donor State

The energy transfer efficiency greatly depends on the process by which the donor state is deactivated, as in the following equation:

$$\eta_{\text{EnT}} = \frac{k_{\text{EnT}}}{k_{\text{EnT}} + k_{\text{R}}(\text{donor}) + k_{\text{NR}}(\text{donor})}. \quad (8)$$

In the case of EuL, the triplet state of the ligand functions as the energy donor to the Eu<sup>3+</sup> ion [4]. The energy donor level in [BMIM][PF<sub>6</sub>] was estimated by acquiring phosphorescence spectra of a gadolinium complex with L (abbreviated as GdL) at 77 K (Figure 4). GdL generates a phosphorescence band at approximately 460 nm in both [BMIM][PF<sub>6</sub>] and the rigid solvent ethanol, as shown in Figure 4.

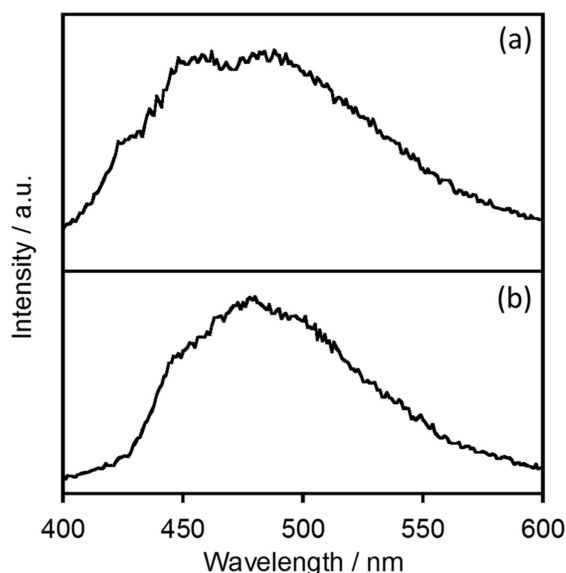


**Figure 4.** Phosphorescence spectra localized on the ligand moiety of helical Gd complex with L in (a) [BMIM][PF<sub>6</sub>] and (b) ethanol at 77 K ( $\lambda_{\text{ex}} = 328 \text{ nm}$ ).

However, the phosphorescence lifetime ( $\tau_{\text{T}}$ ) of GdL in [BMIM][PF<sub>6</sub>] (200 ns) was quite different from that in ethanol (5 ns, Figure S5 and Table 2). Since the phosphorescence quantum yield ( $\phi_{\text{T}}$ ) of

GdL is less than 0.1% in both solvents, the non-radiative rate constant of the triplet state ( $k_{NR}(T)$ ) can be directly approximated by  $\tau_T$  as in the following equations.

$$\phi_T = k_R(T) \times \tau_T = \frac{k_R(T)}{k_R(T) + k_{NR}(T)} < 0.00 \quad (9)$$

$$k_R(T) \ll k_{NR}(T) \quad (10)$$

$$\tau_T = \frac{1}{k_R(T) + k_{NR}(T)} \sim \frac{1}{k_{NR}(T)}. \quad (11)$$

The  $k_{NR}(T)$  value for GdL in [BMIM][PF<sub>6</sub>] is estimated to be  $5.0 \times 10^6 \text{ s}^{-1}$ , which is much smaller than that in methanol ( $2.0 \times 10^8 \text{ s}^{-1}$ ). Thus, the energy transfer from the ligand to the Eu<sup>3+</sup> ion is accelerated in [BMIM][PF<sub>6</sub>] compared to that in organic solvents.

**Table 2.**  $\phi_T$ ,  $\tau_T$ , and  $k_{NR}$  for the triplet state ( $k_{NR}(T)$ ) of the ligand L of helical Gd complex as GdL in [BMIM][PF<sub>6</sub>] and in ethanol at 77 K (<sup>a</sup>:  $\lambda_{ex} = 328 \text{ nm}$ ,  $\lambda_{mon} = 400\text{--}600 \text{ nm}$ , <sup>b</sup>:  $\lambda_{ex} = 340 \text{ nm}$ ,  $\lambda_{mon} = 488 \text{ nm}$ ).

	$\phi_T$ (%) <sup>a</sup>	$\tau_T$ (ns) <sup>b</sup>	$k_{NR}(T)$ (s <sup>-1</sup> )
in [BMIM][PF <sub>6</sub> ]	<0.1	ca. 200	$5.0 \times 10^6$
in ethanol	<0.1	ca. 5	$2.0 \times 10^8$

#### 2.1.4. Effect of the Viscosity of [BMIM][PF<sub>6</sub>] on the Energy Transfer Efficiency of EuL

It is well known that ILs have higher viscosities than organic solvents [26]. The viscosity of solvents may affect the molecular distortion or intermolecular interactions of the Eu complex, which in turn have significant effects on the nonradiative relaxation process, as discussed above. The impact of solvent viscosity on the energy transfer process in EuL was assessed by estimating the rate constants and efficiencies of the energy transfer pathway in mixtures of [BMIM][PF<sub>6</sub>] and acetonitrile with various proportions (Table 3, Figure S3) [27]. The kinetic viscosity of each mixture ( $\nu$ ) will vary with the molar ratio of [BMIM][PF<sub>6</sub>] to acetonitrile. However, the  $\tau_{obs}$ ,  $k_R$ , and  $k_{NR}$  values are independent of the kinetic viscosity, meaning that the ligand field of the Eu<sup>3+</sup> ion is only minimally affected by viscosity. In contrast, the  $\eta_{EnT}$  value is drastically increased at higher viscosities, as shown in Figure 5. It is therefore evident that the more viscous [BMIM][PF<sub>6</sub>] suppresses the nonradiative relaxation of the ligand, as discussed in Section 2.1.2. The result is that the EuL exhibits higher emission efficiency in [BMIM][PF<sub>6</sub>] than in organic solvents.

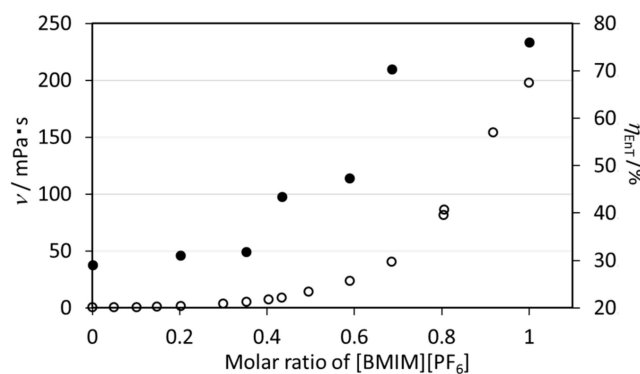


**Figure 5.**  $\eta_{EnT}$  (filled circles) and  $\nu$  (open circles) as functions of the [BMIM][PF<sub>6</sub>] mole fraction.

**Table 3.**  $\phi_{ff}$ ,  $\tau_{obs}$ ,  $n$ ,  $k_R$ ,  $k_{NR}$ , and  $\eta_{EnT}$  values for EuL in mixed solvents of [BMIM][PF<sub>6</sub>] and acetonitrile along with the kinetic viscosity values ( $\nu$ ) [27] (<sup>a</sup>:  $\lambda_{ex}$  = 328 nm,  $\lambda_{mon}$  = 550–780 nm, <sup>b</sup>:  $\lambda_{ex}$  = 340 nm,  $\lambda_{mon}$  = 616 nm).

Molar Ratios [BMIM][PF <sub>6</sub> ]: Acetonitrile		$\nu$ (mPa·s)	$\phi_{ff}$ (%) <sup>a</sup>	$\tau_{obs}$ (ms) <sup>b</sup>	$k_R$ (s <sup>-1</sup> )	$k_{NR}$ (s <sup>-1</sup> )	$\eta_{EnT}$ (%)
1.00	0.00	198.18	32.3	1.46	287.2	388.5	76.0
0.64	0.36	40.69	30.0	1.42	300.7	403.6	70.3
0.59	0.41	23.84	17.6	1.46	254.3	430.6	47.4
0.43	0.75	9.15	15.8	1.43	254.6	444.7	43.4
0.35	0.65	5.31	12.1	1.49	255.2	416.0	31.8
0.20	0.80	1.87	11.6	1.45	257.6	432.0	31.1
0.00	1.00	0.48	12.0	1.55	266.2	379.0	29.1

## 2.2. Temperature Dependence of the Structure and Luminescence Properties of EuL in [EMIM][PF<sub>6</sub>]

### 2.2.1. Luminescence Properties

[EMIM][PF<sub>6</sub>] is a solid at room temperature, as its melting point is around 60 °C. The emission and excitation spectra of EuL dispersed in [EMIM][PF<sub>6</sub>] are shown in Figure 6. In [EMIM][PF<sub>6</sub>], the luminescence bands are observed at the same position as in [BMIM][PF<sub>6</sub>] or acetonitrile. The excitation spectrum acquired in [EMIM][PF<sub>6</sub>] also corresponds to that in [BMIM][PF<sub>6</sub>]. These spectral results indicate that EuL dispersed in [EMIM][PF<sub>6</sub>] does not undergo intramolecular interactions. That is, the molecular structure of EuL is maintained in [EMIM][PF<sub>6</sub>] just as well as in [BMIM][PF<sub>6</sub>]. The  $\phi_{ff}$  value for EuL in [EMIM][PF<sub>6</sub>] is, however, much larger than that in [BMIM][PF<sub>6</sub>] (Table 4) and comparable to that of solid EuL (52.6%) [4]. This increase in  $\phi_{ff}$  results from efficient energy transfer from the ligand to the Eu<sup>3+</sup> ion in [EMIM][PF<sub>6</sub>] ( $\eta_{EnT} > 99\%$ ), since [EMIM][PF<sub>6</sub>] works as a rigid medium and thus mimics the solid state.

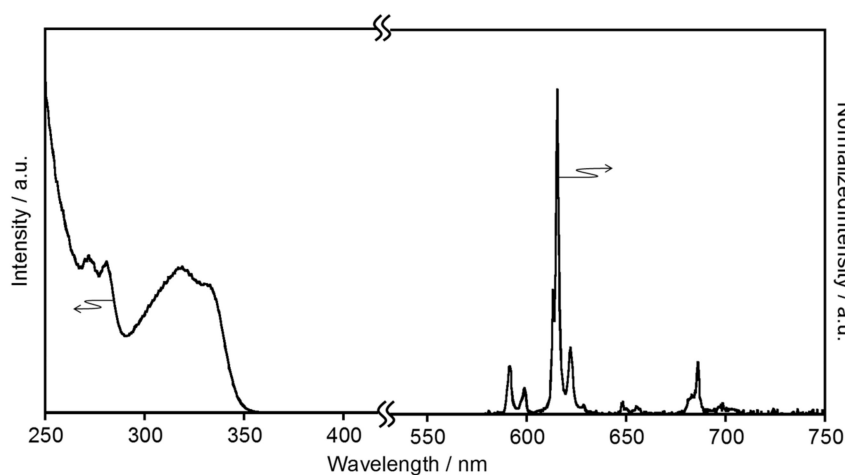


**Figure 6.** Excitation (left) and emission (right) spectra of EuL in [EMIM][PF<sub>6</sub>] ( $\lambda_{mon}$  = 616 nm,  $\lambda_{ex}$  = 328 nm).

**Table 4.**  $\phi_{ff}$ ,  $\tau_{obs}$ , and  $\eta_{EnT}$  values of EuL in [EMIM][PF<sub>6</sub>] (<sup>a</sup>:  $\lambda_{ex}$  = 328 nm,  $\lambda_{mon}$  = 550–782 nm, <sup>b</sup>:  $\lambda_{ex}$  = 340 nm,  $\lambda_{mon}$  = 616 nm).

$\phi_{ff}$ (%) <sup>a</sup>	$\tau_{obs}$ (ms) <sup>b</sup>	$\eta_{EnT}$ (%)
52.1	1.37	>99

### 2.2.2. Structural Analyses

The crystal structure of [EMIM][PF<sub>6</sub>] has already been reported [28] to be monoclinic (space group  $P2_1/c$ ). In this work, synchrotron X-ray powder diffraction (XRPD) analyses of [EMIM][PF<sub>6</sub>] were performed before and after heating, with the results shown in Figure 7a. Diffraction peaks are evident at  $2\theta$  values of 7.6, 9.2, 9.8, 10.8, 12.2, 13.3, 13.7, 13.8, 14.5, 14.7, 15.2, and 15.5° and can be assigned to the (0 1 1), (1 1 0), (1 0 -2), (0 1 2), (1 0 2), (0 0 3), (0 2 1), (2 0 0), (1 2 -2), (2 1 -1), (0 2 2), and (1 2 1) planes, respectively. After re-crystallization of [EMIM][PF<sub>6</sub>] following heating at 70 °C, certain diffraction peaks, such as those for the (1 0 -2), (0 1 2), and (1 0 2) planes, disappear. In these crystal planes (Figure S4a–c), EMIM and PF<sub>6</sub><sup>-</sup> molecules exist in an alternating arrangement. Thus, the disappearance of these crystal planes suggests that the [EMIM][PF<sub>6</sub>] is selectively orientated in the direction of the (0 1 1) and (1 1 0) planes (Figure S4d,e), such that EMIM molecules and PF<sub>6</sub><sup>-</sup> counter anions form separate layers. The diffraction pattern of [EMIM][PF<sub>6</sub>] prior to heating is affected by the addition of EuL (Figure 7b). In addition, following the re-crystallization of [EMIM][PF<sub>6</sub>] containing EuL, the same diffraction peaks disappear. Additionally, the presence of EuL eliminates the (0 1 1) and (1 1 0) diffractions of the [EMIM][PF<sub>6</sub>]. These results indicate that Eu<sup>3+</sup> ions, having a high atomic scattering factor, are readily incorporated into the EMIM or PF<sub>6</sub> layers in conjunction with the re-orientation of the [EMIM][PF<sub>6</sub>].

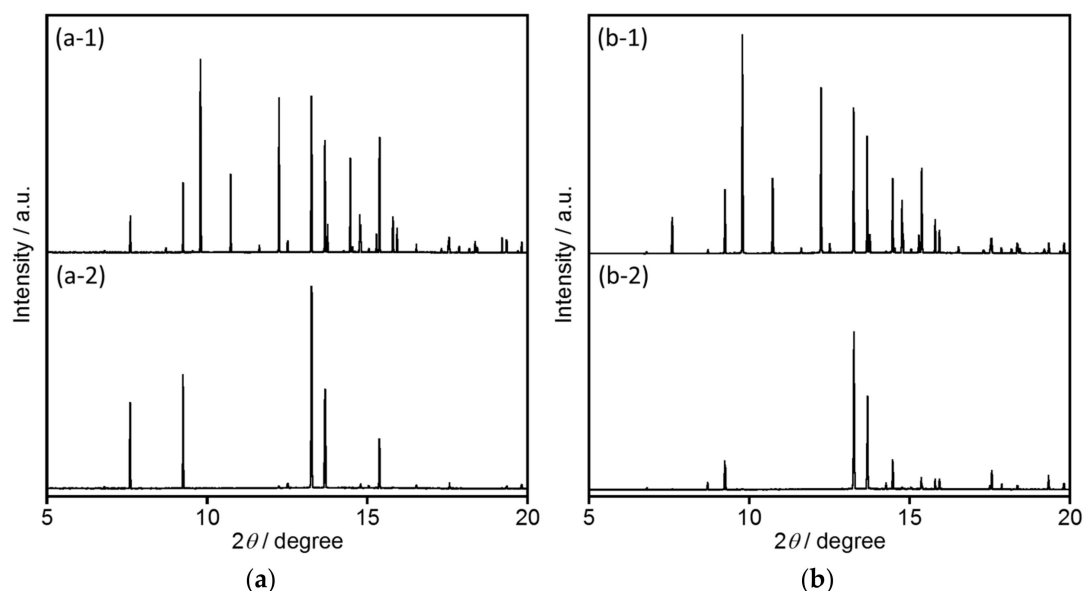


**Figure 7.** Synchrotron X-ray powder diffraction patterns of (a) [EMIM][PF<sub>6</sub>] and (b) EuL in [EMIM][PF<sub>6</sub>]. (a-1,b-1) before and (a-2,b-2) after heating at 70 °C ( $\lambda = 1.017593$  Å).

### 2.2.3. Temperature Dependence of Luminescence Properties

Interestingly, the bright red luminescence of EuL was maintained in [EMIM][PF<sub>6</sub>] even at 120 °C. Figure 8 presents the emission spectra of EuL in [EMIM][PF<sub>6</sub>] at various temperatures and demonstrates very little change in the spectra up to 120 °C. In contrast, in acetonitrile solution, the EuL was decomposed at temperatures above 100 °C such that the emission ceased. It therefore appears that EuL remains in a highly stable structure in [EMIM][PF<sub>6</sub>] even above 100 °C.

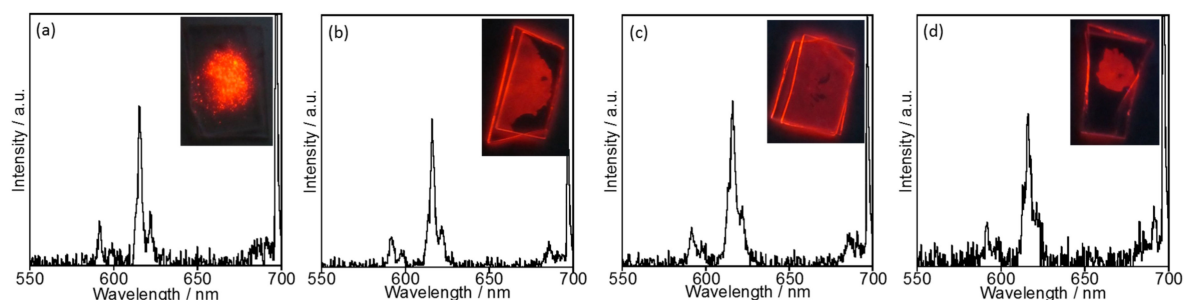


**Figure 8.** In situ temperature dependence of emission spectra with photographs of EuL in [EMIM][PF<sub>6</sub>] at (a) 17, (b) 61, (c) 108, and (d) 121 °C ( $\lambda_{\text{ex}} = 254$  nm).

### 3. Materials and Methods

#### 3.1. Reagents and Materials

The majority of reagents and solvents were used as-received, without further purification from Kanto Chemical Co. Inc. (Tokyo, Japan) and Wako Chemicals (Osaka, Japan). EuL ([Eu(L)(NO<sub>3</sub>)<sub>2</sub>](PF<sub>6</sub>)) was synthesized using a previously reported method [4]. Subsequently, the EuL (0.178  $\mu\text{mol}$ ) was dissolved in [BMIM][PF<sub>6</sub>] (24.2 mmol, approximately 5 mL) and stirred for 10 min at 80 °C to dissolve the complex. Solutions of EuL in [BMIM][PF<sub>6</sub>] and [EMIM][PF<sub>6</sub>] were clear under white light and showed red emission under UV light.

#### 3.2. Measurements

Synchrotron XRPD data were acquired using the large Debye-Scherrer camera installed at the SPring-8 BL02B2 beamline, employing an imaging plate as a detector. The N<sub>2</sub> gas flow system was also installed to allow for low-temperature experiments (down to 77 K).

Electronic absorption and luminescence spectra were recorded on a photo spectrometer UV-3100 Shimadzu (Kyoto, Japan) an absolute specular reflectance attachment and a fluorophoto spectrometer Fluorolog 3–22 Horiba Jobin-Yvon Ltd. (Kyoto, Japan), respectively. Emission decay curves were obtained using a Quantaaurus-tau C11367-12, Hamamatsu Photonics K. K. (Hamamatsu, Japan) with excitation via a xenon flash lamp with a band-path filter ( $\lambda_{\text{ex}} = 340$  nm) and an LED light source for the measurement of ff emission and phosphorescence lifetimes, respectively. The fluorescence quantum yields were determined using a C9920-02 Absolute PL Quantum Yield Measurement System, Hamamatsu Photonics K. K. In situ luminescence spectra at high temperatures were recorded on USB2000 spectrometer equipped with an optical fiber, Ocean Optics Inc. (Dunedin, FL, USA) under UV light.

### 4. Conclusions

We demonstrated that the intramolecular energy transfer in a helical Eu complex (EuL) is accelerated in ILs, resulting in higher emission efficiencies relative to those obtained in organic solvents. The single helical structure of EuL is evidently maintained in both [BMIM][PF<sub>6</sub>] and [EMIM][PF<sub>6</sub>], just as in acetonitrile. EuL in [BMIM][PF<sub>6</sub>] generates bright red luminescence with a quantum yield of 32.3%. This value is significantly greater than that in acetonitrile (12%). Estimations of rate constants associated with energy relaxation show that the energy transfer process is more efficient in [BMIM][PF<sub>6</sub>]. This effect is attributed to the suppression of molecular fluctuations in the ligand. Both the helical structure and strong luminescence of EuL can be maintained in [EMIM][PF<sub>6</sub>] up to 120 °C. To the best of our knowledge, this is the first report of enhanced intramolecular energy transfer in a Eu complex following stabilization of the coordination structure in ILs. These data suggest that the luminescence of various other lanthanide complexes should also be enhanced in ILs.

**Supplementary Materials:** The following are available online. Figure S1: Luminescence decay curves of EuL in [BMIM][PF<sub>6</sub>] and acetonitrile; Figure S2: Excitation spectra of EuL in [BMIM][PF<sub>6</sub>] and in acetonitrile; Figure S3: Electronic absorption, emission spectra, and decay curves of EuL in [BMIM][PF<sub>6</sub>]/acetonitrile; Figure S4: Projection views of a [EMIM][PF<sub>6</sub>] single crystal.

**Acknowledgments:** The authors thank Wolfgang Linert of The Technical University of Vienna and Tomoyuki Mochida of Kobe University for helpful discussions regarding ionic liquids. Synchrotron radiation experiments were performed at the BL02B2 beamline at SPring-8 with the approval of JASRI (Proposal Nos. 2015A1552, 2015A1862, 2015B1353, 2016A1333, 2016A1336, 2016B1342, 2016B1706, 2017A1648, 2017A1380, and 2017B1268). This work was supported by a Grant-in-Aid for Scientific Research on Innovative Areas “Soft Crystals: Area Number 2903” (No. 17H06374, MH) and by the Supported Program for the Strategic Research Foundation at Private Universities (MEXT, MH) via a matching fund subsidy, the Izumi Science Foundation (MH), the Aoyama Gakuin Soken Project (MH), and JST PRESTO (Grant No. JP17941016, AI).

**Author Contributions:** Miki Hasegawa conceived and designed the experiments together with Ayumi Ishii; Yuki Hasegawa, Yudai Inazuka, and Naho Yajima performed the experiments and calculations; Shogo Kawaguchi and Kuniyoshi Sugimoto carried out structural analyses using Synchrotron XRPD. Miki Hasegawa, Ayumi Ishii, Yuki Hasegawa, and Yudai Inazuka wrote the paper.

**Conflicts of Interest:** The authors declare no conflict of interest.

## References

1. Bünzli, J.C.G.; Comby, S.; Chauvin, A.S.; Vandevyver, C.D.B. New Opportunities for Lanthanide Luminescence. *J. Rare Earths* **2007**, *25*, 257–274. [[CrossRef](#)]
2. Bünzli, J.C.G.; Eliseeva, S.V. Intriguing aspects of lanthanide luminescence. *Chem. Sci.* **2013**, *4*, 1939–1949. [[CrossRef](#)]
3. Ogata, S.; Shimizu, T.; Ishibashi, T.; Ishiyone, Y.; Hanami, M.; Ito, M.; Ishii, A.; Kawaguchi, S.; Sugimoto, K.; Hasegawa, M. Water-soluble lanthanide complexes with a helical ligand modified for strong luminescence in a wide pH region. *New J. Chem.* **2017**, *14*, 6385–6394. [[CrossRef](#)]
4. Hasegawa, M.; Ohtsu, H.; Kodama, D.; Kasai, T.; Sakurai, S.; Ishii, A.; Suzuki, K. Luminescence behaviour in acetonitrile and in the solid state of a series of lanthanide complexes with a single helical ligand. *New J. Chem.* **2014**, *38*, 1225–1234. [[CrossRef](#)]
5. Hatanaka, M.; Osawa, A.; Wakabayashi, T.; Morokuma, K.; Hasegawa, M. Computational study on the luminescence quantum yields of terbium complexes with 2,2'-bipyridine derivative ligands. *Phys. Chem. Chem. Phys.* **2017**. [[CrossRef](#)] [[PubMed](#)]
6. Holzweber, M.; Lungwitz, R.; Doerfler, D.; Spange, S.; Koel, M.; Hutter, H.; Linert, W. Mutual Lewis Acid–Base Interactions of Cations and Anions in Ionic Liquids. *Chem. Eur. J.* **2013**, *19*, 288–293. [[CrossRef](#)] [[PubMed](#)]
7. Shimomura, K.; Harami, H.; Matsubara, Y.; Nokami, T.; Katada, N.; Itoh, T. Lipase-mediated dynamic kinetic resolution (DKR) of secondary alcohols in the presence of zeolite using an ionic liquid solvent system. *Catal. Today* **2015**, *255*, 41–48. [[CrossRef](#)]
8. Endo, T.; Kato, T.; Tozaki, K.; Nishikawa, K. Phase behaviors of room temperature ionic liquid linked with cation conformational changes: 1-butyl-3-methylimidazolium hexafluorophosphate. *J. Phys. Chem. B* **2010**, *114*, 407–411. [[CrossRef](#)] [[PubMed](#)]
9. Fukaya, Y.; Hayashi, K.; Wada, M.; Ohno, H. Cellulose dissolution with polar ionic liquids under mild conditions: Required factors for anions. *Green Chem.* **2008**, *10*, 44–46. [[CrossRef](#)]
10. Funasako, Y.; Mori, S.; Mochida, T. Reversible transformation between ionic liquids and coordination polymers by application of light and heat. *Chem. Commun.* **2016**, *52*, 6277–6279. [[CrossRef](#)] [[PubMed](#)]
11. Takao, K.; Takao, S. Efficient and Versatile Anion Metathesis Reaction for Ionic Liquid Preparation by Using Conjugate Acid and Ortho Ester. *Bull. Chem. Soc. Jpn.* **2014**, *87*, 974–981. [[CrossRef](#)]
12. Canales, R.I.; Brennecke, J.F. Comparison of ionic liquids to conventional organic solvents for extraction of aromatics from aliphatics. *J. Chem. Eng. Data* **2016**, *61*, 1685–1699. [[CrossRef](#)]
13. Deferm, C.; de Voorde, M.V.; Luyten, J.; Oosterhof, H.; Fransaer, J.; Binnemans, K. Purification of indium by solvent extraction with undiluted ionic liquids. *Green Chem.* **2016**, *18*, 4116–4127. [[CrossRef](#)]
14. Nockemann, P.; Beurer, E.; Driesen, K.; Deun, R.V.; Hecke, K.V.; Meervelt, L.V.; Binnemans, K. Photostability of a highly luminescent europium  $\beta$ -diketonate complex in imidazolium ionic liquids. *Chem. Commun.* **2005**, *34*, 4354–4356. [[CrossRef](#)] [[PubMed](#)]

15. Driesen, K.; Lunstroot, K.; Nockemann, P.; Hecke, K.V.; Meervelt, L.V.; Gorller-Walrand, C.; Binnemans, K. Visible and near-infrared emission by samarium (III)-containing ionic liquid mixtures. *Inorg. Chem.* **2009**, *48*, 3018–3026.
16. Shobukawa, H.; Tokuda, H.; Tabata, S.; Watanabe, M. Preparation and transport properties of novel lithium ionic liquids. *Electrochim. Acta* **2004**, *50*, 1–5. [[CrossRef](#)]
17. Hayashi, S.; Hamaguchi, H. Discovery of a magnetic ionic liquid [bmim] FeCl<sub>4</sub>. *Chem. Lett.* **2004**, *33*, 1590–1591. [[CrossRef](#)]
18. Welton, T. Room-temperature ionic liquids. Solvents for synthesis and catalysis. *Chem. Rev.* **1999**, *99*, 2071–2083. [[CrossRef](#)] [[PubMed](#)]
19. Hu, Y.; Li, H.; Huang, X.; Chen, L. Novel room temperature molten salt electrolyte based on LiTFSI and acetamide for lithium batteries. *Electrochem. Commun.* **2004**, *6*, 28–32. [[CrossRef](#)]
20. Yi, S.; Wang, J.; Chen, X. Enhanced energy transfer efficiency and stability of europium  $\beta$ -diketonate complex in ionic liquid-based lyotropic liquid crystals. *Phys. Chem. Chem. Phys.* **2015**, *17*, 20322–20330. [[CrossRef](#)] [[PubMed](#)]
21. Kabo, G.J.; Blokhin, A.V.; Paulechka, Y.U.; Kabo, A.G.; Shymanovich, M.P. Thermodynamic properties of 1-butyl-3-methylimidazolium hexafluorophosphate in the condensed state. *J. Chem. Eng. Data* **2004**, *49*, 453–461. [[CrossRef](#)]
22. Fuller, J.; Carlin, R.T.; De Long, H.C.; Haworth, D. Structure of 1-ethyl-3-methylimidazolium hexafluorophosphate: Model for room temperature molten salts. *J. Chem. Soc. Chem. Commun.* **1994**, *3*, 299–300. [[CrossRef](#)]
23. Huddleston, J.G.; Visser, A.E.; Reichert, W.M.; Willauer, H.D.; Broker, G.A.; Rogers, R.D. Characterization and comparison of hydrophilic and hydrophobic room temperature ionic liquids incorporating the imidazolium cation. *Green Chem.* **2001**, *3*, 156–164. [[CrossRef](#)]
24. Reichardt, C. *Solvents and Solvent Effects in Organic Chemistry*, 2nd ed.; VCH: New York, NY, USA, 1988; pp. 365–371.
25. Carnall, W.T.; Fields, P.T.; Rajnak, K. Electronic energy levels of the trivalent lanthanide aquo ions. IV. Eu<sup>3+</sup>. *J. Chem. Phys.* **1968**, *49*, 4450–4455. [[CrossRef](#)]
26. Frez, C.; Diebold, G.J.; Tran, C.D.; Yu, S. Determination of thermal diffusivities, thermal conductivities, and sound speeds of room-temperature ionic liquids by the transient grating technique. *J. Chem. Eng. Data* **2006**, *51*, 1250–1255. [[CrossRef](#)]
27. Moattar, M.T.Z.; Cegincara, R.M. Viscosity, density, speed of sound, and refractive index of binary mixtures of organic solvent+ ionic liquid, 1-butyl-3-methylimidazolium hexafluorophosphate at 298.15 K. *J. Chem. Eng. Data* **2007**, *52*, 2359–2364. [[CrossRef](#)]
28. Reichert, W.M.; Holbrey, J.D.; Swatloski, R.P.; Gutowski, K.E.; Visser, A.E.; Nieuwenhuyzen, M.; Seddon, K.R.; Rogers, R.D. Solid-state analysis of low-melting 1, 3-dialkylimidazolium hexafluorophosphate salts (ionic liquids) by combined X-ray crystallographic and computational analyses. *Cryst. Growth Des.* **2007**, *7*, 1106–1114. [[CrossRef](#)]

**Sample Availability:** Samples of the compounds are available from the authors.



© 2018 by the authors. Licensee MDPI, Basel, Switzerland. This article is an open access article distributed under the terms and conditions of the Creative Commons Attribution (CC BY) license (<http://creativecommons.org/licenses/by/4.0/>).